Inorg. Chem. **2004**, *43*, 6075–6082

Ferromagnetic Anomaly Associated with the Antiferromagnetic Transitions in (Donor)[Ni(mnt)$_2$]-Type Charge-Transfer Salts

Hideyasu Nakajima, Mao Katsuhara, Minoru Ashizawa, Tadashi Kawamoto, and Takehiko Mori*

Department of Organic and Polymeric Materials, Graduate School of Science and Engineering, Tokyo Institute of Technology, O-okayama, Meguro-ku, Tokyo 152-8552, Japan

Received March 15, 2004

Three newly prepared [Ni(mnt)$_2$] complexes, (HMTTF)[Ni(mnt)$_2$], (ChSTF)[Ni(mnt)$_2$], and (DBTTF)$_2$[Ni(mnt)$_2$], are reported (DBTTF = dibenzotetrathiafulvalene, ChSTF = 2,3-cyclohexylenedithio-1,4-dithia-5,8-diselanafulvalene, HMTTF = bis(trimethylene)-tetrathiafulvalene, and mnt = maleonitrile dithiolate). The former two compounds have usual DA-type (D = donor, A = acceptor) mixed stacks, whereas the DBTTF complex has DDDDAA-type 6-fold columns. These compounds are electrical insulators, but the HMTTF and ChSTF complexes exhibit χT minima at 16 and 55 K, respectively, followed by χT peaks at 8 and 16 K. Below these temperatures the ESR signal disappears, indicating antiferromagnetic transitions. The origin of the ferromagnetic interaction is explained either from the difference of the *g* values between the donor and the anion or from the intrinsic ferromagnetic interaction of the [Ni(mnt)$_2$] anions.

Introduction

In the past few decades, a considerable number of molecular ferromagnets, such as metal−tetracyanoethylenes[1] and *p*-nitronil nitroxides,[2] have been prepared.[3] Among them, ferrimagnetic materials composed of two kinds of metal atoms,[4] or, alternatively, one kind of metal atom and organic radicals,[5] construct an important family. In this analogy, several molecular ferrimagnets have been found in charge-transfer salts between TTF-type organic donors and metal complexes; representatives are (TTF)[Cr(NCS)$_4$(phen)] and (BEDT-TTF)[Cr(NCS)$_4$(isoq)$_2$] (TTF = tetrathiafulvalene, BEDT-TTF = bis(ethlenedithio)-TTF, phen = phenantroline, and isoq = isoquinoline).[6] In these materials, the donor has a 1^+ charge and $S = {}^1/_2$ spin and the anion has a 1^- charge so that the d^3 Cr has $S = {}^3/_2$ spin. Accordingly, the alternating stack of the donor and the anion gives rise to ferrimagnetic spin order around 4−9 K. The Cr atom is, however, octahedrally coordinated, and the anion is nonplanar so that the donors and the anions are not in a mixed stack in the usual manner. Though there are face-to-face contacts between the organic donor and π ligands such as isoquinoline, the πd interactions are mainly mediated by the NCS sulfur atoms.[7]

These findings have prompted us to investigate the magnetic interactions in simpler charge-transfer complexes composed of planar anions such as [Ni(mnt)$_2$]$^-$ (mnt = maleonitrile dithiolate). Although the charge-transfer complexes of [Ni(mnt)$_2$]$^-$ with organic donors have been investigated for a long time,[8] not many have been structurally

* Author to whom correspondence should be addressed. E-mail: takehiko@o.cc.titech.ac.jp.

(1) (a) Miller, J. S.; Calabrese, J. C.; Rommelmann, H.; Chittipeddi, S. R.; Zhang, J. H.; Reiff, W. M.; Epstein, A. J. *J. Am. Chem. Soc*. **1987**, *109*, 769. (b) Manriquez, J. M.; Yee, G. T.; McLean, R. S.; Epstein, A. J.; Miller, J. S. *Science* **1991**, *252*, 1415. (c) Allemand, P. M.; Khemani, K. C.; Koch, A.; Wudl, F.; Holczer, K.; Donovan, S.; Grüner, G.; Thompson, J. D. *Science* **1991**, *253*, 302.

(2) Tamura, M.; Nakazawa, D.; Shiomi, D.; Nozawa, K.; Hosokoshi, Y.; Ishikawa, M.; Takahashi, M.; Kinoshita, M. *Chem. Phys. Lett*. **1991**, *186*, 401.

(3) (a) Kahn, O. *Molecular Magnetism*; VCH: Weinheim, Germany, 1993. (b) *Magnetism: Molecules to Matrials I*−*IV*; Miller, J. S., Drillon, M., Eds.; VCH: Weinheim, Germany, 2002.

(4) (a) Kahn, O.; Pei, M.; Verdague, M.; Renard, J. P.; Sletten, J. *J. Am. Chem. Soc*. **1988**, *110*, 782. (b) Ohba, M.; Okawa, H. *Coord. Chem. Rev*. **2000**, *198*, 313.

(5) (a) Caneschi, A.; Gatteschi, D.; Ray, P. *Prog. Inorg. Chem*. **1991**, *39*, 331. (b) Inoue, K.; Iwahori, F.; Markosyan, A. S.; Iwamura, H. *Coord. Chem. Rev*. **2000**, *198*, 219.

(6) (a) Turner, S. S.; Michaut, C.; Durot, S.; Day, P.; Gelbrich, T.; Hursthouse, M. B. *J. Chem. Soc., Dalton Trans*. **2000**, 905. (b) Turner, S. S.; Pevelen, D. L.; Day, P.; Prout, K. *J. Chem. Soc., Dalton Trans*. **2000**, 2739. (c) Setifi, F.; Golhen, S.; Ouahab, L.; Turner, S. S.; Day, P. *CrystEngComm* **2002**, *4*, 1. (d) Setifi, F.; Golhen, S.; Ouahab, L.; Miyazaki, A.; Okabe, K.; Enoki, T.; Tita, T.; Yamada, J. *Inorg. Chem*. **2002**, *41*, 3786.

(7) (a) Mori, T.; Katsuhara M. *J. Phys. Soc. Jpn*. **2003**, *72*, 149. (b) Katsuhara M.; Mori, T. Submitted for publication.

(8) (a) Wudl, F. *J. Am. Chem. Soc*. **1975**, *97*, 1962. (b) Miles, M. G.; Wilson, J. D.; *Inorg. Chem*. **1975**, *14*, 2357. (c) Underhill, A. E.; Tonge, J. S.; Clemenson, P. I.; Wang, H. H.; Williams, J. M. *Mol. Cryst. Liq. Cryst*. **1985**, *125*, 439.

10.1021/ic049670m CCC: $27.50
Published on Web 08/20/2004

and magnetically well identified. The crystal structures of $(TTF)_2[Ni(mnt)_2]$ and (BEDT-TTF)$[Ni(mnt)_2]$ are known, but the physical properties are not reported.[9] $(Perylene)_2$-$[M(mnt)_2]$ (M = Fe, Co, Ni, Cu, Pd, and Pt) have segregate stacks and are metals down to relatively low temperatures (58, 73, 32, 25, and 15 K for the Fe, Co, Ni, Cu, and Pt complexes, respectively),[10] whereas the magnetic susceptibility, even of the paramagnetic anions (Fe and Ni), drops to zero at low temperatures accompanied by the lattice distortion.[10c−e] $(BMDT\text{-}TTF)_2[M(mnt)_2]$ and (EDT-TTF)-$[M(mnt)_2]$ have mixed stacks, but the magnetic susceptibility follows the usual one-dimensional antiferromagnetic model (BMDT-TTF = bis(methylenedithio-TTF, and EDT-TTF = ethylenedithio-TTF).[11] The magnetic susceptibility of mix-stacked $(EDT\text{-}TTFI_2)_2[M(mnt)_2]$ also follows the usual antiferromagnetic model (EDT-$TTFI_2$ = diiodoethylene-dithio-TTF).[12] By contrast, (BDNT)$[M(mnt)_2]$ (M = Ni, Pd, Pt, and Au) show relatively high conductivity (1 S/cm), and the Ni complex exhibits ferromagnetic interaction (J/k_B = 3.4 K according to the one-dimensional ferromagnetic model), but the crystal structure is unknown (BDNT = 4,5-bis(1,3-benzodithiol-2-ylidene)-4,9-dihydronaphtho [2,3-*c*]-[1,2,5]thiadiazole).[13] (EDO-$TTFI_2$)$[M(mnt)_2]$ (M = Ni and Pt) have segregated columns with metallic conductivity above 110 K, whereas the magnetic susceptibility shows ferromagnetic interaction (the Weiss temperatures are 14 and 15 K for the Ni and Pt complexes, respectively), and the Pt complex undergoes an antiferromagnetic transition at 5.5 K (EDO-$TTFI_2$ = diiodoethylenedioxy-TTF).[14] The origin of the ferromagnetic interaction is ascribed to the interaction of the anions following MacConnell's first model.[15] These previous results seem to show that a ferromagnetic interaction is observed in relatively highly conducting materials (probably) having segregated stacks, and the mix-stacked compounds exhibit the usual antiferromagnetic interaction.

The present work reports structures and properties of three newly prepared $[Ni(mnt)_2]$ complexes: (HMTTF)$[Ni(mnt)_2]$, (ChSTF)$[Ni(mnt)_2]$, and $(DBTTF)_2[Ni(mnt)_2]$. Although all of these compounds are mix-stacked insulators, the former two compounds show strong ferromagnetic interactions above the antiferromagnetic transitions.

Scheme 1

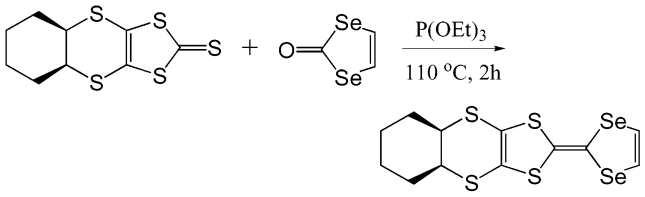

Experimental Section

Because ChSTF is a new donor, we briefly describe the synthesis. The synthesis of ChSTF (**3**) was carried out by using a triethylphosphite-mediated coupling reaction of 4,5-cyclohexylenedithio-1,3-dithiole -2-thione (**1**)[16] and 1,3-diselenol-2-ketone (**2**)[17] (Scheme 1). Compounds **1** (0.76 g, 2.7 mmol) and **2** (0.40 g, 1.9 mmol) were heated at 110 °C in triethyl phosphite (10 mL) for 2 h. After the mixture was cooled to room temperature, the solvent was removed in vacuo and purified by column chromatography (silica gel, CS_2) to afford ChSTF (**3**) (0.52 g, 62%), as an orange solid. ^{1}H NMR ($CDCl_3$) δ 1.45−1.98 (8H, m), 2.62 (2H, m), 7.20 (2H, s); MS *m*/*z* 444 (M^+, 100%), 442 ($M^+ - 2$, 98%).

In cyclic voltammetry, this donor showed two redox waves up to dications. The first redox potential, $E^1_{1/2}$, was 0.38 V and the second one, $E^2_{1/2}$, was 0.77 V, so $E^2_{1/2} - E^1_{1/2}$, which is a measure of the on-site Coulomb repulsion, was 0.39 V (measured in benzonitrile in the presence of *n*-Bu_4NPF_6 as a supporting electrolyte using a carbon glass working electrode and a Pt counter electrode with a Ag^+/AgCl reference electrode at 25 °C). These values were comparable to $E^1_{1/2}$ = 0.37 V and $E^2_{1/2}$ = 0.81 V for BEDT-TTF measured under the identical conditions. The other donors were prepared according to the literature.[18]

Crystals were grown by electrochemical oxidation in CH_2Cl_2 in the presence of the donor and $Bu_4N[Ni(mnt)_2]$ using an H-shaped cell equipped with Pt electrodes. A constant current of 1.0−1.2 μA was applied at room temperature, and after one week, black blocks were harvested.

The X-ray diffraction measurements were performed on a Rigaku four-circle diffractometer AFC-7R with graphite monochromatized Mo Kα radiation ($2\theta < 60°$) for HMTTF and ChSTF salts, and an R-AXIS CS imaging plate for the DBTTF salt. The structures were solved by the direct method (SIR97).[19] The structures were refined by the full-matrix least squares procedure by applying anisotropic temperature factors for all non-hydrogen atoms. Crystallographic data are summarized in Table 1, and the selected bond lengths are listed in Table 2. Atomic coordinates and further details of crystal structure results were deposited as Supporting Information. Intermolecular overlap integrals between the HOMO of the donors and the LUMO of the acceptors were calculated on the basis of the extended Hückel molecular orbital calculations.[7]

Electrical resistivity was measured by the usual four-probe method using 15-μm gold wire and carbon paint. Magnetic

(9) (a) Mahadevan, C. *J. Crystallogr. Spectrosc. Res*. **1986**, *16*, 159. (b) Reith, W.; Polborn, K.; Amberger, E. *Angew. Chem., Int. Ed. Engl*. **1988**, *27*, 699.
(10) (a) Alcacer, L.; Maki, A. H. *J. Phys. Chem*. **1974**, *78*, 215. (b) Alcacer, L.; Novais, H.; Pedroso, F.; Flandrois, S.; Coulon, C.; Chasseau, D.; Gaultier, J. *Solid State Commun*. **1980**, *35*, 945. (c) Gama, V.; Almeida, M.; Hendriques, R. T.; Santos, I. C.; Domingos, A.; Ravy, S.; Pouget, J. P. *J. Phys. Chem.* **1991**, *95*, 4263. (d) Gama, V.; Hendriques, R. T.; Bonfait, G.; Pereira, L. C.; Warenborgh, J. C.; Santos, I. C.; Duarte, M. T.; Cabral, J. M. P.; Almeida, M. *Inorg. Chem*. **1992**, *31*, 2598. (e) Gama, V.; Hendriques, R. T.; Almeida, M.; Bourdonnais, C.; Pouget, J. P.; Jerome, D.; Auban-Senzier, P.; Gotschy, B. *J. Phys. I* **1993**, *3*, 1235. (f) Gama, V.; Hendriques, R. T.; Almeida, M. *J. Phys. Chem.* **1994**, *98*, 997.
(11) Mas-Torrent, M.; Alves, H.; Lopes, E. B.; Almeida, M.; Wurst, K.; Vidal-Gancedo, J.; Veciana, J.; Rovira, C. *J. Solid State Chem*. **2002**, *168*, 563.
(12) Devic, T.; Domercq, B.; Auban-Senizier, P.; Molinié, P.; Fourmigue, M. *Eur. J. Inorg. Chem*. **2002**, 2844.
(13) Uruichi, M.; Yakushi, K.; Yamashita, Y.; Qin, J. *J. Mater. Chem*. **1998**, *8*, 141.
(14) (a) Nishijo, J.; Ogura, E.; Yamaura, J.; Miyazaki, A.; Enoki, T.; Takano, T.; Kuwatani, Y.; Iyoda, M. *Solid State Commun*. **2000**, *116*, 661. (b) Miyazaki, A.; Enomoto, K.; Okabe, K. Yamazaki, H.; Nishijo, J.; Enoki, T.; Ogura, E.; Ugawa, K.; Kuwatani, Y.; Iyoda, M. *J. Solid State Chem*. **2002**, *168*, 547.
(15) McConnell, H. M. *J. Chem. Phys*. **1963**, *39*, 1910.
(16) Svenstrup, N.; Becher, J. *Synthesis* **1995**, 215.
(17) Takimiya, K.; Morikami, A.; Otsubo, T. *Synlett* **1997**, 319.
(18) (a) Gerard, L. C.; Yves, M. *J. Chem. Soc., Chem. Commun.* **1980**, *1*, 38. (b) Spencer, H. K.; Cava, M. P.; Yamagishi, F. G.; Garito, A. F. *J. Org. Chem.* **1976**, *41*, 730. (c) Morand, J. P.; Brzezinski, L.; Manigand, C. *J. Chem. Soc., Chem Commun*. **1986**, *13*, 1050.
(19) Altomare, A.; Cascrano, M.; Giacovazzo, C.; Guagiliardi, A. *J. Appl. Crystallogr*. **1993**, *26*, 343.

Table 1. Crystallographic Data of (HMTTF)[Ni(mnt)$_2$] (ChSTF)[Ni(mnt)$_2$], and (DBTTF)$_2$[Ni(mnt)$_2$]

	(HMTTF)[Ni(mnt)$_2$]	(ChSTF)[Ni(mnt)$_2$]	(DBTTF)$_2$[Ni(mnt)$_2$]
chemical formula	$C_{20}H_{12}N_4NiS_8$	$C_{20}H_{12}N_4NiS_8Se_2$	$C_{36}H_{16}N_4NiS_{12}$
fw	623.52	781.44	948.02
shape	black block	black block	black block
cryst syst	triclinic	triclinic	triclinic
space group	$P\bar{1}$	$P\bar{1}$	$P\bar{1}$
a/Å	7.878(2)	9.071(8)	13.555(6)
b/Å	13.391(2)	24.69(4)	15.445(7)
c/Å	5.9288(9)	6.081(4)	10.352(5)
α/deg	96.37(1)	89.39(8)	106.19(5)
β/deg	98.09(2)	106.44(6)	102.39(5)
γ/deg	105.10(2)	90.4(1)	109.14(4)
V/Å^3	590.7(2)	1305(2)	1851(1)
Z	1	2	2
D_{calcd}/g cm^{-3}	1.753	1.987	1.700
λ/Å	0.71069	0.71069	0.71070
T/K	298	298	195
R1[a]	0.044	0.083	0.067
wR2[b]	0.134	0.227	0.157
reflns	3444	7650	7894

[a] $R1 = \sum||F_o| - |F_c||/\sum|F_o|$. [b] $wR2 = [\sum w(|F_o| - |F_c|)^2/\sum wF_o^2]^{1/2}$.

susceptibilities were measured using a Quantum Design MPMS-5 SQUID magnetometer down to 1.8 K. ESR spectra were recorded with a JEOL TE-100 spectrometer equipped with a Scientific Instrument ES-CT470 continuous flow helium cryostat. For the SQUID and ESR measurements, nonoriented microcrystalline samples were used for the HMTTF complex, whereas a single crystal was used for the ChSTF complex.

Results

Crystal Structures. Crystallographic data of (HMTTF)[Ni(mnt)$_2$] (ChSTF)[Ni(mnt)$_2$], and (DBTTF)$_2$[Ni(mnt)$_2$] are listed in Table 1. ORTEP drawings of the molecular structure with the atomic numbering scheme are shown in Figure 1.

An asymmetric unit of (HMTTF)[Ni(mnt)$_2$] contains half of the donor and half of the anion molecules, both lying on inversion centers (Figure 2). When the average Ni−S distance, 2.143 Å, (Table 2) is compared with the previous results,[11] the charge on [Ni(mnt)$_2$] is expected to be 1$^-$. The bond lengths of the donor, particularly of the central C(6)═C(6) bond, 1.406(7) Å, and of the average C−S bond, 1.724 Å, also support the donor charge, 1$^+$.[20] The donor and acceptor molecules are alternately stacked along the crystallographic a axis (Figure 2a), and the stacking axis is not perpendicular to the molecular plane; it forms an angle of about 65° with the molecular plane (Table 3). In this sense, the structure is close to the β'' phase rather than the β phase, known in radical-cation salts. As listed in Table 3, the calculated intermolecular overlap integrals between the HOMO of the donor and the LUMO of the acceptor are large both for the a and c directions.[7] The alignment of the same kind of molecules, namely the DD interaction and the AA interaction (D = donor, A = acceptor), runs in the 34° direction with respect to the molecular plane (along the c axis). In particular, the DD interaction (c1) in this direction is very large. The interactions in the 65° and 0° directions are DA interactions.

(ChSTF)$_2$[Ni(mnt)$_2$] contains one crystallographically independent ChSTF molecule and one anion, which are located on general positions. Although the lattice constants are close to monoclinic, attempts to solve the structure under monoclinic space groups are unsuccessful. This is not surprising because in the final results, all molecules are parallel to each other, and there are no 2, 2$_1$, mirror, or glide symmetries. The cyclohexane ring of the donor has a chair conformation, but the thermal motion is considerably large (Figure 1b). The donor and acceptor molecules are alternately stacked along the a axis (Figure 3a). The stacking axis again forms an angle of 64° with respect to the molecular plane. Among the calculated intermolecular overlap integrals (Table 3), the DD interaction (c1) is again largest, but there are considerable interactions in the three (a: 64°, c: 35°, and p: 0°) directions.

An asymmetric unit of (DBTTF)$_2$[Ni(mnt)$_2$] includes two donor molecules and one anion molecule, both lying on general positions so that the composition is 2:1. The average Ni−S distance indicates a 1$^-$ charge, and the central C═C bond lengths, 1.352(4) Å for donor A and 1.394(5) Å for donor B, together with the average C−S lengths, 1.759 Å for A and 1.732 Å for B, indicate charge disproportionation as 0 and 1$^+$ (Table 2). The donor and anion molecules construct a mixed stack along the $a + 2c$ axis (Figure 4), and six molecules form the repeating unit $A^0B^+B^+A^0C^-C^-$. The anion molecules are then dimerized, and the donors are tetramerized. The stacking axis is 70° from the molecular plane. The 2:1 composition and the resulting nonsimple mixed-stacking structure may be related to the weak donor ability of DBTTF.[21]

Physical Properties. Owing to the mixed stack structures, these complexes are electrical insulators; the room temperature resistivity is 1.9×10^6 Ω cm for the ChSTF complex.

Magnetic properties of (HMTTF)[Ni(mnt)$_2$] have been measured for nonoriented polycrystalline samples. The ESR

(20) Legros, J.-P.; Bousseau, M.; Valade, L.; Cassoux, P. *Mol. Cryst. Liq. Cryst*. **1983**, *100*, 181.

(21) Hünig, S.; Kieblich, G.; Quast, H.; Scheutzow, D. *Liebigs Ann. Chem*. **1973**, 310.

Table 2. Selected Bond Lengths (Å) of (HMTTF)[Ni(mnt)$_2$], (ChSTF)[Ni(mnt)$_2$], and (DBTTF)$_2$[Ni(mnt)$_2$]

	(HMTTF)[Ni(mnt)$_2$]		
Ni(1)−S(3)	2.1386(9)	Ni(1)−S(4)	2.1477(9)
S(1)−C(4)	1.723(4)	S(1)−C(6)	1.727(4)
S(3)−C(9)	1.713(4)	S(4)−C(10)	1.710(4)
N(1)−C(7)	1.140(5)	N(2)−C(8)	1.131(5)
C(1)−C(2)	1.539(6)	C(1)−C(3)	1.526(6)
C(2)−C(4)	1.499(5)	C(3)−C(5)	1.499(5)
C(4)−C(5)	1.344(5)	C(6)−C(6)	1.406(7)
C(7)−C(9)	1.425(5)	C(8)−C(10)	1.435(5)
C(9)−C(10)	1.737(5)		
	(ChSTF)[Ni(mnt)$_2$]		
Ni(1)−S(5)	2.141(3)	Ni(1)−S(6)	2.135(3)
Ni(1)−S(7)	2.137(3)	Ni(1)−S(6)	2.146(3)
Se(1)−C(10)	1.89(1)	Se(1)−C(11)	1.86(1)
Se(2)−C(10)	1.86(1)	Se(2)−C(12)	1.84(1)
S(1)−C(5)	1.70(1)	S(1)−C(7)	1.74(1)
S(2)−C(6)	2.02(1)	S(2)−C(8)	1.73(1)
S(3)−C(7)	1.72(1)	S(3)−C(9)	1.74(1)
S(4)−C(8)	1.726(1)	S(4)−C(9)	1.71(1)
S(5)−C(15)	1.71(1)	S(5)−C(16)	1.71(1)
S(6)−C(16)	1.70(1)	S(7)−C(17)	1.71(1)
S(8)−C(18)	1.71(1)	N(1)−C(13)	1.14(1)
N(2)−C(14)	1.15(1)	N(3)−C(19)	1.17(1)
N(4)−C(20)	1.16(1)	C(1)−C(2)	1.61(3)
C(1)−C(3)	1.38(3)	C(2)−C(3)	1.91(4)
C(2)−C(4)	1.80(3)	C(3)−C(5)	1.80(2)
C(4)−C(5)	1.90(3)	C(4)−C(6)	1.21(4)
C(5)−C(6)	1.38(1)	C(7)−C(8)	1.36(1)
C(9)−C(10)	1.35(1)	C(11)−C(12)	1.36(1)
C(13)−C(15)	1.43(1)	C(14)−C(16)	1.40(1)
C(15)−C(16)	1.40(1)	C(17)−C(18)	1.38(1)
C(17)−C(19)	1.43(1)	C(18)−C(20)	1.42(1)
	(DBTTF)$_2$[Ni(mnt)$_2$]		
Ni(1)−S(9)	2.153(1)	Ni(1)−S(10)	2.155(1)
Ni(1)−S(11)	2.150(2)	Ni(1)−S(12)	2.158(1)
S(1)−C(5)	1.747(3)	S(1)−C(7)	1.760(4)
S(2)−C(6)	1.755(3)	S(2)−C(7)	1.758(3)
S(3)−C(8)	1.754(3)	S(3)−C(9)	1.749(4)
S(4)−C(8)	1.765(3)	S(4)−C(10)	1.765(4)
S(5)−C(19)	1.743(3)	S(5)−C(21)	1.741(3)
S(6)−C(20)	1.749(3)	S(6)−C(21)	1.725(3)
S(7)−C(22)	1.730(3)	S(7)−C(23)	1.738(3)
S(8)−C(22)	1.730(3)	S(8)−C(24)	1.748(3)
S(9)−C(31)	1.725(3)	S(10)−C(32)	1.715(3)
S(11)−C(33)	1.724(4)	S(12)−C(34)	1.721(3)
N(1)−C(29)	1.144(5)	N(2)−C(30)	1.146(5)
N(3)−C(35)	1.141(5)	N(4)−C(36)	1.147(5)
C(1)−C(2)	1.384(5)	C(1)−C(3)	1.389(5)
C(2)−C(4)	1.389(5)	C(3)−C(5)	1.388(5)
C(4)−C(6)	1.391(5)	C(5)−C(6)	1.416(4)
C(7)−C(8)	1.352(4)	C(9)−C(10)	1.405(5)
C(9)−C(11)	1.400(5)	C(10)−C(12)	1.395(5)
C(11)−C(13)	1.386(6)	C(12)−C(14)	1.385(5)
C(13)−C(14)	1.393(6)	C(15)−C(16)	1.411(5)
C(15)−C(17)	1.384(5)	C(16)−C(18)	1.379(5)
C(17)−C(19)	1.393(4)	C(18)−C(20)	1.398(4)
C(19)−C(20)	1.418(4)	C(21)−C(22)	1.394(5)
C(23)−C(24)	1.411(5)	C(23)−C(25)	1.416(4)
C(24)−C(26)	1.386(4)	C(25)−C(27)	1.373(5)
C(26)−C(28)	1.381(5)	C(27)−C(28)	1.409(5)
C(29)−C(31)	1.439(5)	C(30)−C(32)	1.441(5)
C(31)−C(32)	1.375(4)	C(33)−C(34)	1.384(5)
C(33)−C(35)	1.431(5)	C(34)−C(36)	1.436(5)

spectra of the HMTTF and the ChSTF complexes give a single Lorenzian in the whole temperature range without separating the donor and the anion spins, indicating the presence of exchange interaction between these spins. Figure 5 shows the temperature dependence of the *g* value, the peak-to-peak line width, and the intensity for the HMTTF salt. The *g* value is 2.030 at room temperature, which is greater

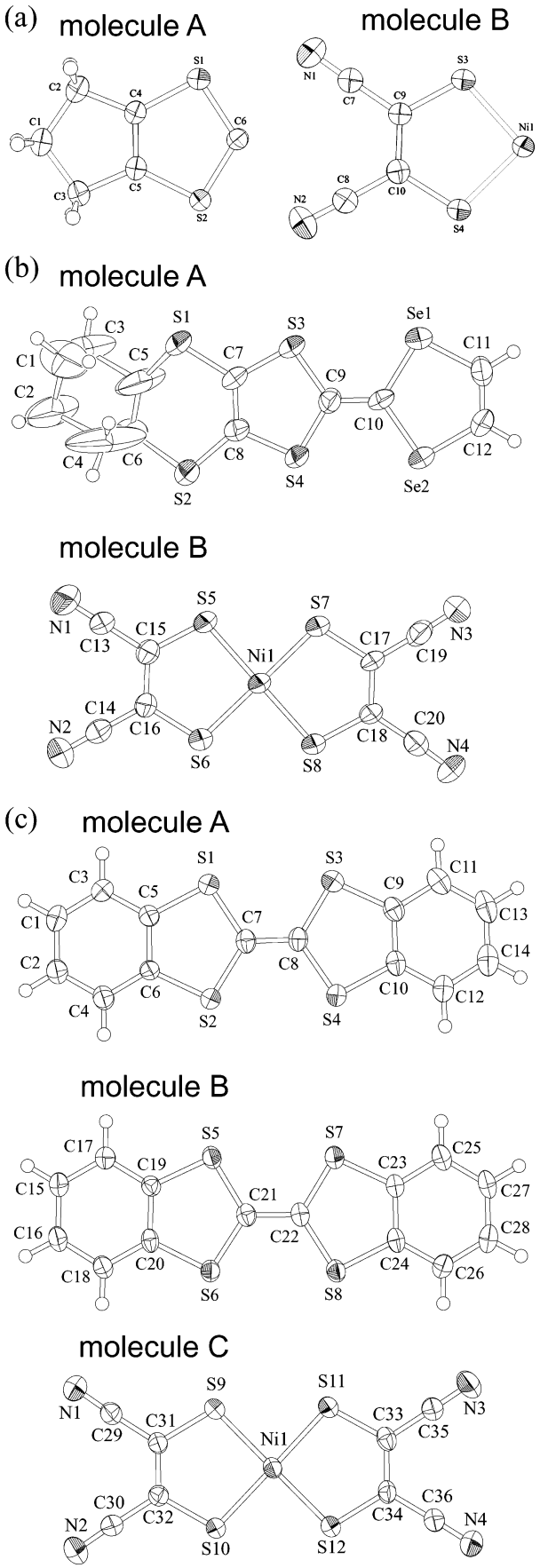

Figure 1. ORTEP drawings with the atomic numbering scheme of (a) HMTTF and [Ni(mnt)$_2$] in (HMTTF)[Ni(mnt)$_2$], (b) ChSTF and [Ni(mnt)$_2$] in (ChSTF)[Ni(mnt)$_2$], and (c) DBTTF and [Ni(mnt)$_2$] in (DBTTF)$_2$[Ni(mnt)$_2$].

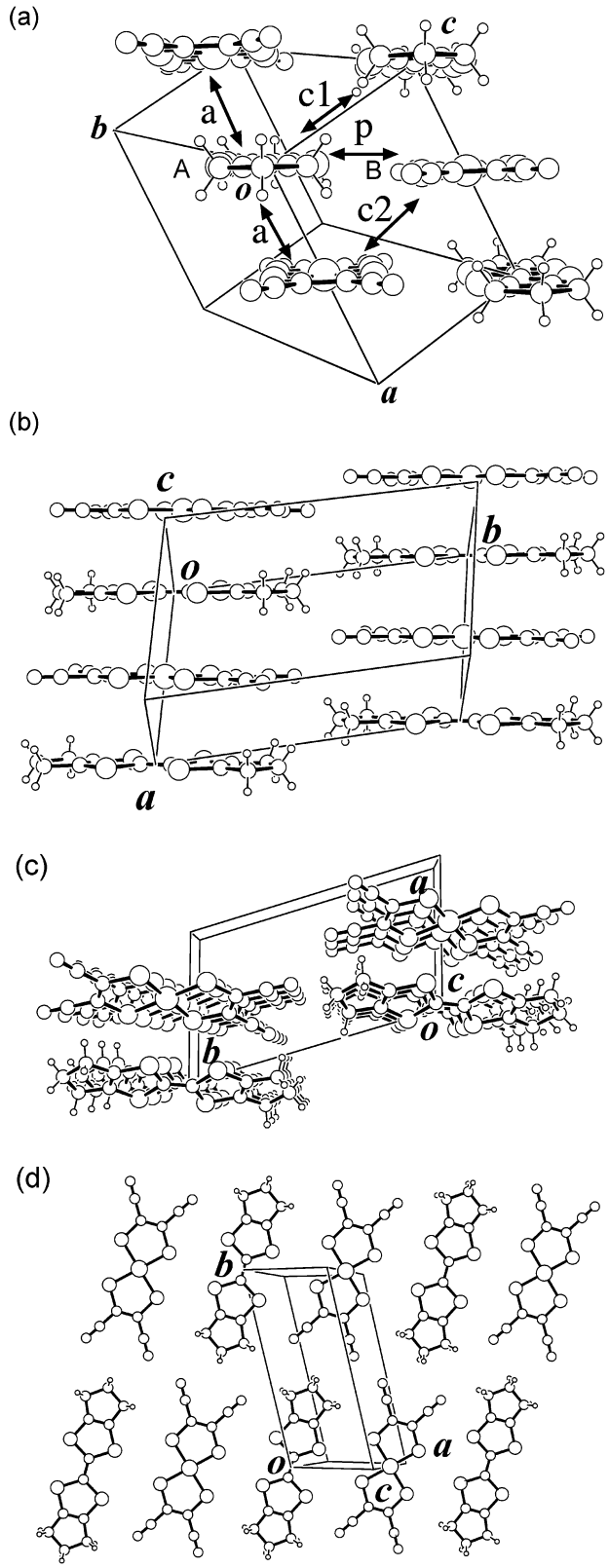

Figure 2. Crystal structure of (HMTTF)[Ni(mnt)$_2$]. (a) View along the molecular long axis, (b) view along the short axis, (c) view along the crystallographic *c* axis, and (d) view perpendicular to the molecular plane.

than $g_{max} = 2.011$ for TTF donors,[22] indicating that the contribution from [Ni(mnt)$_2$] is included.[13] This is also

(22) Sugano, T.; Saito, G.; Kinoshita, M. *Phys. Rev. B* **1986**, *34*, 117.

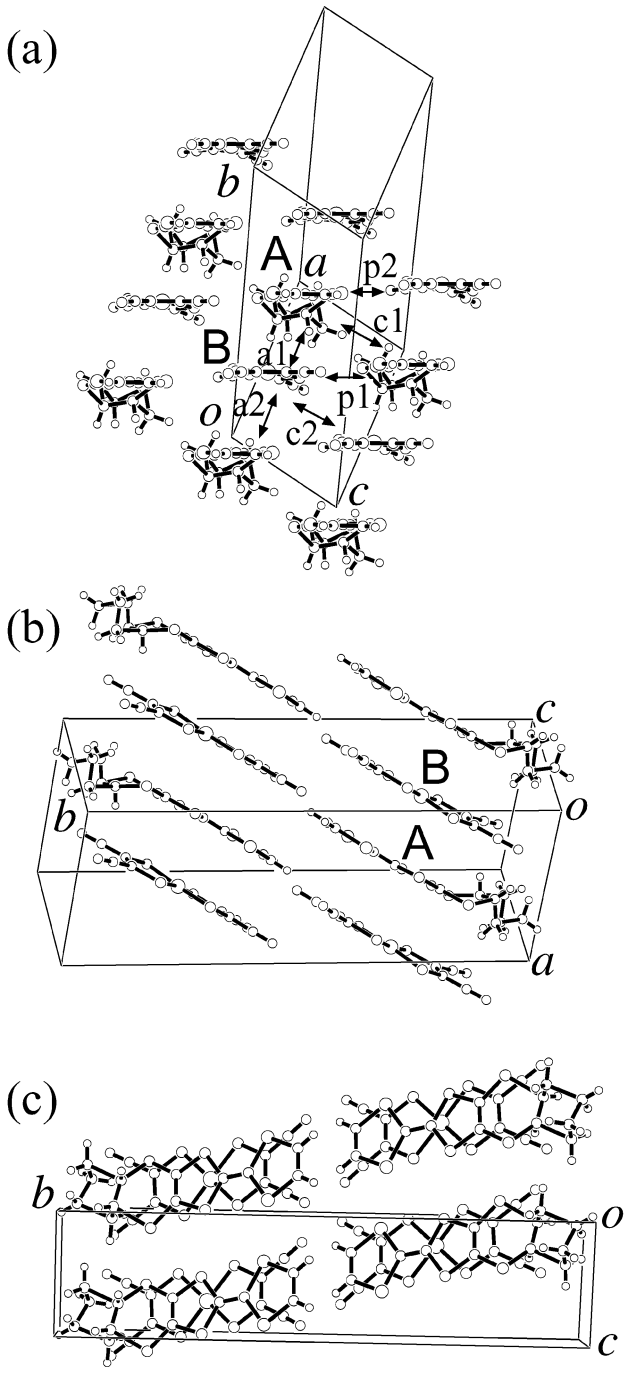

Figure 3. Crystal structure of (ChSTF)[Ni(mnt)$_2$]. (a) View along the molecular long axis, (b) view along the short axis, and (c) view along the crystallographic *a* axis.

Table 3. Calculated Overlap Integrals *S*, and the Angle of the Intermolecular Direction from the Molecular Plane ϕ

(HMTTF)[Ni(mnt)$_2$]				(ChSTF)[Ni(mnt)$_2$]			
mode		$S/10^{-3}$	ϕ/deg	mode		$S/10^{-3}$	ϕ/deg
a	DA	−6.8	65	a1	DA	−2.6	64
				a2	DA	−2.5	63
c1	DD	−12.8	34	c1	DD	−12.2	35
c2	AA	2.5	34	c2	AA	2.1	35
p	DA	−0.9	3	p1	DA	−3.2	3
				p2	DA	−1.4	3

supported by the relatively large line width (60 mT at room temperature). The intensity is nearly constant from room

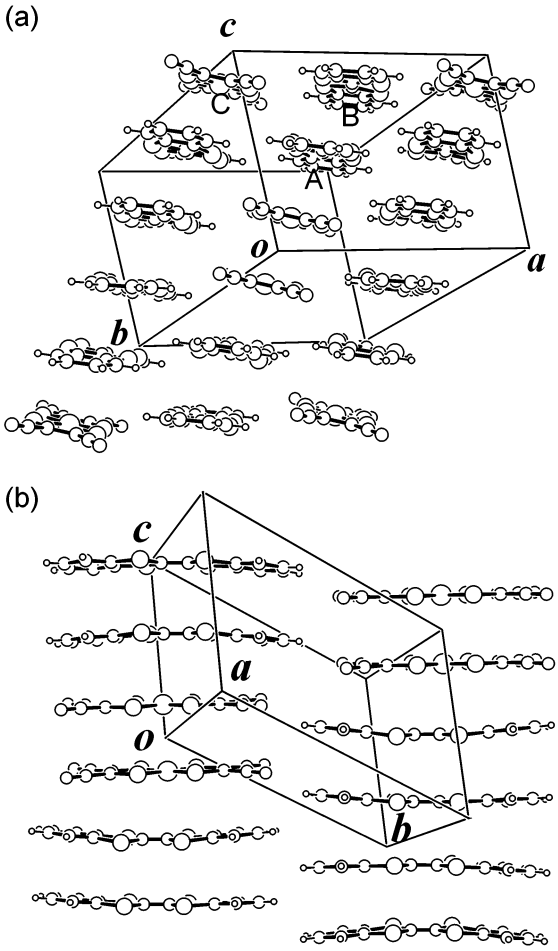

Figure 4. Crystal structure of $(DBTTF)_2[Ni(mnt)_2]$. (a) View along the molecular long axis and (b) view along the short axis.

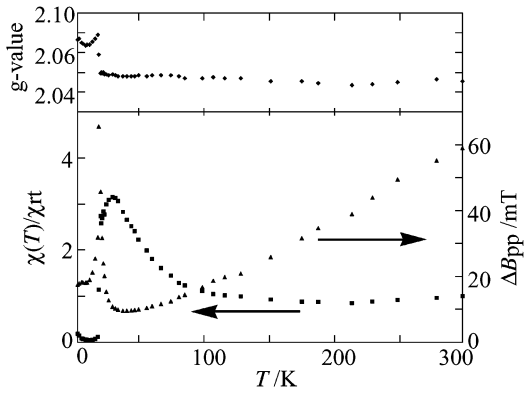

Figure 5. Temperature dependence of the ESR g value, the peak-to-peak line width, and the intensity for $(HMTTF)[Ni(mnt)_2]$.

temperature to 100 K and gradually increases down to 30 K. In this temperature range, the g value is almost constant, and the line width decreases monotonically. The intensity makes a peak around 30 K and rapidly drops below this temperature, accompanied by abrupt broadening of the line width. This indicates a magnetic transition around this temperature. It is noteworthy that the g value considerably increases below this transition.

The temperature dependence of the static susceptibility is shown in Figure 6. The susceptibility obeys the Curie−Weiss law at high temperatures, where the Curie constant is 0.70

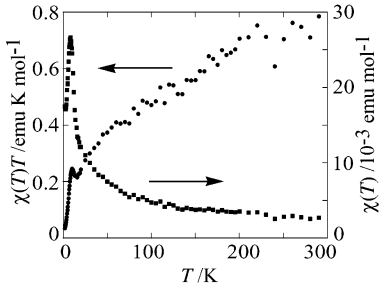

Figure 6. Temperature dependence of the static susceptibility χ and χT of $(HMTTF)[Ni(mnt)_2]$.

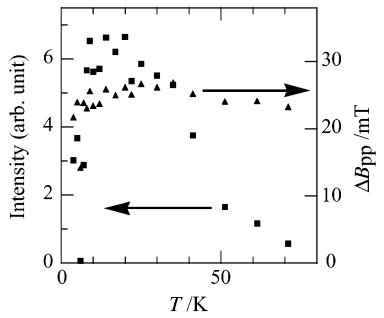

Figure 7. Temperature dependence of the ESR peak-to-peak line width and the intensity for $(ChSTF)[Ni(mnt)_2]$. The magnetic field is applied along the crystallographic $a-c$ axis.

emu K mol^{-1} and the Weiss temperature is −30 K. The observed Curie constant is consistent with the spin-only value of two $S = 1/2$ spins, $0.375 \times 2 = 0.75$ emu K mol^{-1}. The relatively large Weiss temperature indicates the presence of large antiferromagnetic interactions. It is noteworthy that the susceptibility follows the Curie−Weiss law rather than low-dimensional models. This is reasonable because the calculated overlap integrals (Table 3) do not show one-dimensionality.

The susceptibility exhibits a rapid increase below 20 K and makes a sharp peak at 8 K. Below this temperature, the susceptibility drops sharply. The susceptibility at 2 K is about two-thirds of the peak value, indicating an antiferromagnetic phase measured for a nonoriented sample. Even the χT plot makes a minimum around 16 K and forms a peak around 8 K, suggesting some kind of ferromagnetic interaction.

The temperature dependence of the ESR peak-to-peak line width and the intensity for $(ChSTF)[Ni(mnt)_2]$ are shown in Figure 7. The g value is about 2.055, indicating the contribution of the $[Ni(mnt)_2]$ anion. The ESR spectra are recorded only below 80 K because the signal rapidly diminishes above this temperature. The line width does not change much below this temperature. The intensity increases considerably and makes a maximum around 10−20 K. The ESR signal disappears below 9 K, though the broadening of the line width is not clear in this compound. This suggests some kind of magnetic ordering, and in analogy with the HMTTF compound, this is probably an antiferromagnetic transition.

The temperature dependence of the static susceptibility is shown in Figure 8. The high-temperature static susceptibility follows the Curie−Weiss law with the Curie constant, 0.65 emu K mol^{-1}, and the Weiss temperature, −7 K. The χT

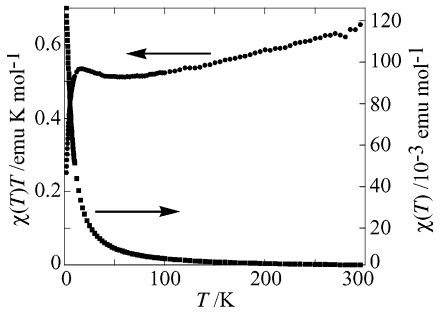

Figure 8. The temperature dependence of static χ and χT for (ChSTF)[Ni(mnt)$_2$]. The magnetic field is applied along the $a-c$ axis.

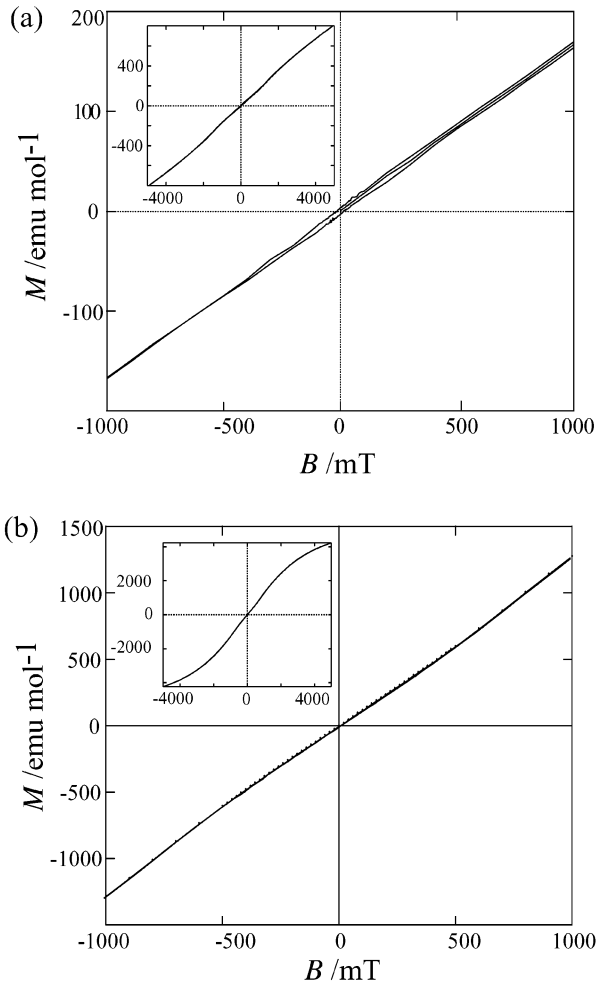

Figure 9. Magnetization versus applied field at 2 K for (a) (HMTTF)[Ni(mnt)$_2$] and (b) (ChSTF)[Ni(mnt)$_2$]. The crystals are randomly oriented in part a, and oriented so as to make the stacking axis parallel to the magnetic field in part b.

plot shows a minimum around 55 K and makes a peak around 16 K. The susceptibility does not show a clear drop, but χT rapidly drops below $T_N = 9$ K. Although the static susceptibility does not provide clear evidence of magnetic transition, the result does not conflict with the magnetic transition observed in the ESR measurement.

Figure 9 shows the magnetization curve at low temperature. Although the magnetization curve shows very weak saturation, the curve of the HMTTF complex shows inflection points around 1.4 T, associated with a spin-flop transition. At low fields, a small hysteresis is observed for the HMTTF complex. This reminds us that induced weak ferromagnetism was observed in (C_1TESe-TTF)$FeBr_4$.[23] The magnetization curve of the ChSTF complex is more usual, probably because no clear anomaly has been observed in the χT results (Figure 8) at this temperature.

The DBTTF complex is expected to be diamagnetic on account of the dimerized structure.

Discussion

Both the ESR and the static susceptibility of (HMTTF)[Ni(mnt)$_2$] clearly show the antiferromagnetic transition. The transition temperature observed in ESR, 20 K, is, however, considerably higher than that of the static susceptibility, 10 K. Below 20 K, the ESR g value increases considerably (Figure 5). This increase seems to coincide with the χT peak (Figure 6). Because χT should be proportional to g^2, the χT peak is explained by the g shift. If the spins of the mix-stacked chain align antiferromagnetically, then all donors have upward spins and all anion spins are downward. Although both the donor and the anion have $S = {}^1/_2$ spin, the spin lengths are slightly different, and the difference, measured by the difference of the g values, brings about the χT peak. This is similar to the χT peak observed in one-dimensional ferrimagnetic chains such as (TTF)[Cr(NCS)$_4$(phen)],[6] where χT shows a slight decrease from room temperature to low temperature, makes a minimum, and exhibits a giant increase coming from the ferrimagnetic intrachain order, followed by a rapid drop associated with an antiferromagnetic transition. The peaks observed in the present compounds are not so large because S is the same for the donor and the anion. The 20 K anomaly observed in ESR is attributed to a short-range antiferomagnetic order in the mix-stacked chain, and the 10 K transition in the static susceptibility is ascribed to the three-dimensional antiferromagnetic transition.

This interpretation seems to be very plausible, but ferromagnetic interaction has been observed in other [M(mnt)$_2$] complexes such as (EDO-TTFI_2)[M(mnt)$_2$] (M = Ni and Pt) and (BDNT)[Ni(mnt)$_2$],[13,14] which probably have segregated [Ni(mnt)$_2$] columns. In addition, ferromagnetic order has been reported in NH_4[Ni(mnt)$_2$](H_2O).[24] These compounds suggest that the [Ni(mnt)$_2$] molecules tend to afford ferromagnetic interactions by themselves. This has been attributed to MacConnell's first model.[15] The present compounds have anion−anion interactions in the 30° direction (Table 3), and ferromagnetic interaction in this direction is another possible origin of the observed ferromagnetic anomaly.

The present compounds are, however, the first mix-stacked compounds showing ferromagnetic interaction, and all other mixed-stacked materials such as (BMDT-TTF)$_2$[M(mnt)$_2$], (EDT-TTF)[M(mnt)$_2$], and (EDT-TTFI_2)$_2$[M(mnt)$_2$] exhibit usual antiferromagnetic interactions.[11,12] Thus, it still remains enigmatic why only the present compounds show ferromag-

(23) Enomoto, M.; Miyazaki, A.; Enoki, T. *Mol. Cryst. Liq. Cryst. Sci. Technol.* **1999**, *335*, 293.
(24) Coomber, A. T.; Beljonne, D.; Friend, R. H.; Bredas, J. L.; Charlton, A.; Robertson, N.; Underhill, A. E.; Kurmoo, M.; Day, P. *Nature* **1996**, *380*, 144.

netic anomalies. More systematic study of the same kind of compounds will resolve these points.

Acknowledgment. We are grateful to Prof. T. Enoki for pointing out the analogy of the anomalous magnetization with (C_1TESe-TTF)$FeBr_4$. This work was partly supported by a Grant-in-Aid for Scientific Research on Priority Areas of Molecular Conductors (no. 15073211) from the Ministry of Education, Culture, Sports, Science and Technology, Japan.

Supporting Information Available: Crystallographic data in CIF format. This material is available free of charge via the Internet at http://pubs.acs.org.

IC049670M